International Journal of Hydrogen Energy 146 (2025) 149891

Contents lists available at ScienceDirect

International Journal of Hydrogen Energy

journal homepage: www.elsevier.com/locate/he

# Drive mechanisms and hydrogen recovery in underground storage: a material balance and simulation approach

Ibrahim A. Alobaidan *, Branko Bijeljic, Martin J. Blunt

*Department of Earth Science and Engineering, Imperial College, London, UK*

ARTICLE INFO

*Keywords:*
Underground hydrogen storage
Gas expansion
Water influx
Exsolution
Rock compressibility

ABSTRACT

Investigating the primary drive mechanisms in underground hydrogen storage (UHS) is crucial for optimizing hydrogen recovery from geological formations. In this study, we used a 3D heterogeneous geological model to assess the dynamics of hydrogen storage in an aquifer under various hydrodynamic and geological conditions, using material balance to quantify the contribution of different production mechanisms including gas expansion, water influx, exsolution, and the compressibility of rock and water. Our findings indicate that gas expansion and rock compressibility are the predominant mechanisms driving hydrogen recovery for closed boundary conditions with minimal aquifer support, whereas water influx dominates when there is substantial aquifer connectivity. Exsolution as a driving force has a negligible impact on hydrogen recovery, simplifying the modelling of storage dynamics. Furthermore, cushion gas injection was found to notably improve gas expansion under open boundary conditions, optimizing hydrogen recovery during the initial production phases. The study underscores the influence of uncertain parameters and processes on hydrogen storage efficiency, offering critical insights for the design of UHS and identifying key reservoir and fluid properties necessary for robust management.

## 1. Introduction

The global energy transition is driven by the urgent need to address climate change. This shift requires a significant reduction in reliance on traditional fossil fuels and a rapid increase in the adoption of renewable energy sources. However, this transition presents challenges in maintaining grid stability and ensuring a reliable energy supply. A promising solution to these challenges is the use of hydrogen, produced from surplus renewable energy, as an energy carrier. Hydrogen can be stored in large quantities in aquifers and depleted hydrocarbon reservoirs, making underground hydrogen storage (UHS) a critical component of a sustainable energy future. UHS addresses the intermittency of renewable energy sources and supports global efforts to mitigate climate change.

Despite the potential of UHS, our understanding of hydrogen behaviour and interactions within subsurface porous media remains limited [1–4]. Given hydrogen's distinct characteristics compared to methane and $CO_2$, as well as reservoir properties and the cyclic operations inherent in UHS, several challenges must be addressed. These involve accounting for multiphase fluid flow in porous media, including trapping, mixing with other gases, and biogeochemical reactions. According to Ref. [4], understanding the complex multiphase displacement patterns, which are influenced by fluid and rock properties, and the relationships between fluid saturation and relative permeability, are crucial for UHS operations. Hydrogen's low viscosity and high diffusivity in brine-filled porous media create uncertainties in flow behaviour, as high mobility can cause viscous fingering and trap hydrogen in unrecoverable pockets [4,5]. The works referenced in Refs. [6–8] discuss the mixing of gaseous components influenced by factors such as mobility ratio, density difference, molecular diffusion, and mechanical dispersion. According to Refs. [1,4], biogeochemical reactions may lead to contamination of stored hydrogen by other gases (e.g., hydrogen sulphide), changes in injectivity due to mineral dissolution or precipitation, formation of migration pathways through the caprock, and alterations in the mechanical properties of the reservoir and caprock.

Recently, several simulation studies have delved into evaluating the feasibility of UHS. These studies, as summarized in Table 1, have considered depleted hydrocarbon reservoirs and aquifers, exploring various aspects crucial for effective implementation. They have studied four main areas: geological parameters (depth, thickness, porosity, geothermal gradient, structural shape, and dip angle); operational parameters (injection and withdrawal rates, cycling frequency, well configurations, cushion gas injection strategies); flow behaviour

* Corresponding author. Department of Earth Science & Engineering, Imperial College London, Prince Consort Road, London, SW7 2BP, UK.
*E-mail addresses:* ibrahim.alobaidan21@imperial.ac.uk (I.A. Alobaidan), b.bijeljic@imperial.ac.uk (B. Bijeljic), m.blunt@imperial.ac.uk (M.J. Blunt).

https://doi.org/10.1016/j.ijhydene.2025.06.081
Received 29 November 2024; Received in revised form 30 May 2025; Accepted 4 June 2025
Available online 17 June 2025
0360-3199/© 2025 The Authors. Published by Elsevier Ltd on behalf of Hydrogen Energy Publications LLC. This is an open access article under the CC BY license (http://creativecommons.org/licenses/by/4.0/).

(permeability, relative permeability hysteresis and wettability); and gas mixing (types of cushion gas, effect of temperature, solubility, diffusivity, hydrogen purity and reactions). Traditional reservoir engineering principles initially developed for hydrocarbon fields have been adapted to manage and evaluate storage performance. Nevertheless, the limited availability of representative core- and field-scale data is a recurring challenge that could potentially constrain the broader applicability of the findings.

In contrast, the study of drive mechanisms in the context of UHS has received very little attention. Drive mechanisms refer to the physical processes that provide the energy required for moving fluids within a reservoir towards production wells. Investigating these mechanisms is essential for developing effective management strategies to optimize storage performance. In conventional oil and gas fields, drive mechanisms—such as gas expansion, water influx, and solution gas drive—have been extensively studied and characterized in the literature [9–11]. While UHS draws on this foundational understanding, the behaviour of hydrogen introduces new complexities due to its distinct physical and chemical characteristics. Nevertheless, several drive mechanisms are expected to be active in UHS, namely: gas expansion, water influx, exsolution, and the compressibility of both rock and water. These are identified from established reservoir engineering principles and illustrated in Fig. 1. These mechanisms govern pressure support, hydrogen recovery, and overall storage performance. A key operational difference, however, is that hydrogen needs to be both injected and produced, while the timescales are shorter: injection and retrieval need to be on a seasonal basis, rather than having slow pressure decline over decades.

Gas expansion (GE) serves as a primary drive mechanism for the recovery of subsurface fluids, especially in high-quality, high-permeability reservoirs with limited water influx. The expansion process results from either an increase in temperature or a decrease in pressure, causing the gas volume to expand. During production, gas expands, displacing resident fluids and driving them towards production wells. This effect can be significant since hydrogen has a higher compressibility compared to other gases under similar conditions. According to Ref. [12], at the pore-scale, hydrogen accesses more of the larger pores by expansion than by injection. This characteristic presents an opportunity to enhance hydrogen recovery in UHS through gas expansion, which could increase the average gas saturation by approximately 20 % as pressure declines [12].

Another important mechanism is water influx (WI) from an adjacent aquifer, which could effectively moderate pressure fluctuations during storage and retrieval [10,11]. During injection, the aquifer can facilitate water displacement from the storage zone and enable its return during production to maintain stable pressure levels. The extent to which water influx enhances gas recovery depends on the aquifer's size, the degree of connectivity between the aquifer and the storage volume, and the volume of water encroaching on the storage zone [10]. Analytical aquifer models such as Carter-Tracy [13] or Fetkovich [14] can be used to model water influx and outflow from the storage zone.

Other effects include exsolution (EX), rock compressibility (RC), and water compressibility (WC). Exsolution refers to the process in which gas dissolved in formation water is released as reservoir pressure declines, once the pressure falls below the gas's solubility limit. This behaviour is well established in conventional reservoirs, where pressure depletion leads to the emergence of a separate gas phase from the liquid [10,11]. Although hydrogen's solubility in pure water is relatively low [15], this mechanism could still contribute to recovery when hydrogen is stored in aquifers or water-saturated gas reservoirs. As pressure decreases, dissolved hydrogen is liberated from the aqueous phase and transitions into a free gas phase. The newly liberated hydrogen then joins the existing free gas in the storage zone, effectively increasing the total hydrogen volume available for recovery.

Rock compressibility refers to the slight expansion or contraction of the formation rock itself as fluid pressure decreases or increases, respectively. While generally small, this effect can impact gas recovery, particularly in tight reservoirs where other drive mechanisms are less effective. Rock compressibility becomes significant over large reservoir volumes and contributes to reservoir drive, especially at high pressures [10,11].

On the other hand, water compressibility within the storage formation usually makes only a small contribution to recovery. This is more significant for large storage volumes with a high initial water saturation [10,11].

The primary aim of this study is to evaluate the contributions of various drive mechanisms to hydrogen recovery from underground storage within an aquifer, using material balance and numerical simulations. This helps identify key controlling parameters, supporting effective reservoir appraisal and production management. We utilize a 3D heterogeneous geological model [16] and incorporate representative fluid and rock properties from the literature [17]. Two contrasting

**Table 1**
A summary of recent field-scale UHS simulation studies and key information.

| Ref. | Storage type | Simulator | Equation of state | Relative permeability, $k_r$ | Consider $k_r$ hysteresis? | Consider solubility? | Cushion gas |
|---|---|---|---|---|---|---|---|
| [18] | Saline aquifer | CMG GEM | SRK | $H_2$-water [19] | No | No | |
| [20] | Depleted gas reservoir | ECLIPSE E300 | PR | $H_2$-water [19] | No | Yes | $CH_4$ |
| [21] | Depleted oil reservoir | CMG GEM | | Oil-water and gas-oil | No | Yes | $CH_4$, $CO_2$, $N_2$ |
| [22] | Depleted oil reservoir and saline aquifer | CMG GEM | PR | Oil-water and gas-oil | No | Yes | $CH_4$ |
| [23] | Depleted gas reservoir | Tough + RealGasBrine | SRK | The modified Stone's model [24] | No | Yes | $N_2$, $CO_2$ |
| [25] | Aquifer | CMG GEM | PR | $H_2$-water [19] | Yes | Yes | |
| [26] | Aquifer | CMG GEM | PR | $H_2$-water [27] | Yes | No | $N_2$ |
| [8] | Aquifer | DARSim | GERG-2008 [28] | $H_2$-water [19] | No | Yes | $CH_4$, $CO_2$, $N_2$ |
| [29] | Offshore aquifer | ECLIPSE E100 | | $H_2$-water [17] | Yes | No | $H_2$ |
| [30] | Depleted gas reservoir | CMG GEM | PR | $H_2$-water [31] | Yes | | $H_2$ |
| [32] | Aquifer | CMG GEM | PR | $H_2$-water [19] | Yes | Yes | $CH_4$, $CO_2$ |
| [33] | Aquifer | CMG IMEX | | $H_2$-water [19] | Yes | No | |
| [34] | Aquifer | CMG GEM | PR | $H_2$-water [19] | Yes | Yes | $CH_4$, $CO_2$, $N_2$ |
| [35] | Saline aquifer | PetraSim + TOUGH3 | | $H_2$-water [17,31] | Yes | | |

ˆ SRK: Soave-Redlich-Kowng (1972) [36].
ˆ PR: Peng-Robinson (1976) [37].

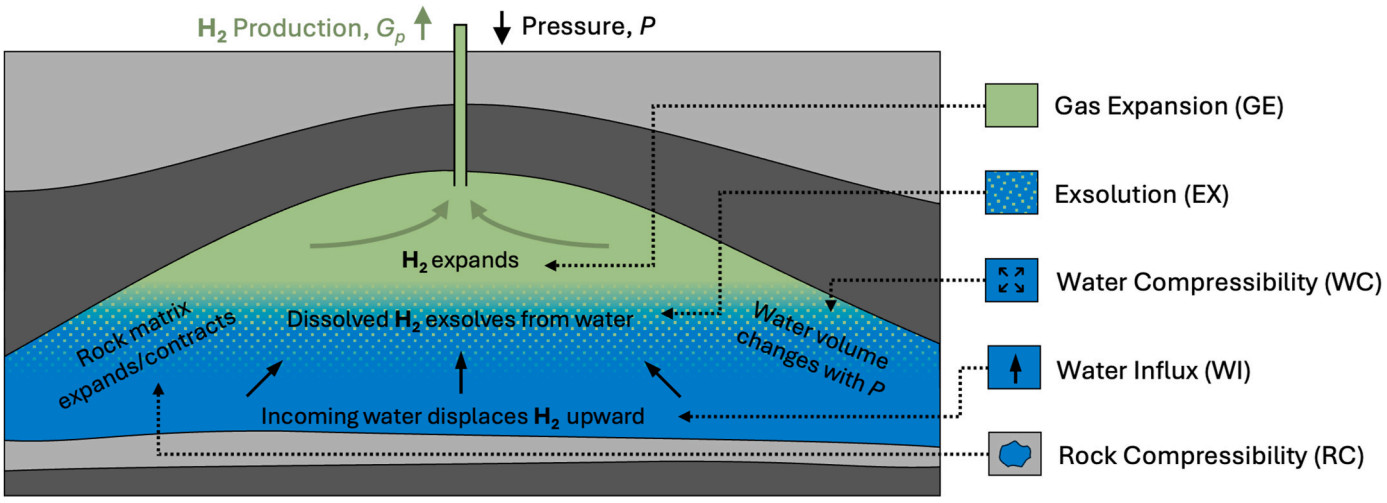



**Fig. 1.** Conceptual schematic illustrating the drive mechanisms involved in hydrogen recovery from underground storage. As pressure declines during production, hydrogen expands and flows toward the well, water influx from surrounding formations displaces hydrogen upwards, dissolved hydrogen exsolves from formation water, and both rock and water compressibility contribute to pressure support. These processes act simultaneously within the storage formation and collectively influence hydrogen recovery.

scenarios were selected to represent a realistic range of subsurface conditions affecting hydrogen recovery: closed boundaries with no active aquifer support (Case A) and open boundaries with active aquifer support (Case B). Case A reflects a fully confined storage configuration, such as one bounded by impermeable faults, while Case B represents a setting with strong water influx from a well-connected aquifer. Together, they define the operational extremes for evaluating hydrogen recovery performance. A material balance equation tailored for UHS will be derived, validated against simulation results, and applied to quantify recovery contributions across multiple storage cycles using dimensionless recovery indices. Sensitivity analyses will then be conducted to evaluate the impact of key processes and uncertain parameters on recovery mechanisms, specifically examining the effects of solubility, rock compressibility, cushion gas and hysteresis. The findings will provide guidelines to identify the critical parameters and uncertainties for the assessment of hydrogen storage, dependent on the dominant recovery processes.

## 2. Material balance

Traditionally, contributions from various drive mechanisms are assessed through material balance, a fundamental principle in reservoir engineering that focuses on tracking mass and converting between reservoir and surface conditions [9]. This robust approach not only aids in identifying primary drive mechanisms but also serves as a predictive tool for recovery potential, using production and pressure data as key inputs. Each of these mechanisms is integral to deriving the material balance equation (MBE) and contributes to the overall hydrogen production. The general form of the MBE for gas production, $G_p$, from underground storage can be expressed as:

$$G_p = G_{GE} + G_{WI} + G_{EX} + G_{RC} + G_{WC} \tag{1}$$

Each term, representing a surface gas volume contributing to the overall production, is derived based on the established material balance approach used in reservoir engineering [9,10]. The gas expansion term, $G_{GE}$, represents the volume of hydrogen produced due to gas expansion:

$$G_{GE} = G_i\left(1 - \frac{B_{gi}}{B_g}\right) \tag{2}$$

where $G_i$ [m$^3$] is the initial free gas in place before production measured at surface conditions, $B_{gi}$ is the initial gas formation volume factor (the ratio of reservoir to surface volumes) and $B_g$ is the gas formation volume factor at any given time during production.

The term $G_{WI}$ accounts for the aquifer water influx, $W_e$, from an adjacent aquifer, displacing hydrogen towards the production well:

$$G_{WI} = \frac{W_e}{B_g} = \frac{G_i B_{gi}}{B_g}\left(1 - \frac{S_g}{S_{gi}}\right) \tag{3}$$

where $S_{gi}$ is the initial gas saturation before production in the storage zone and $S_g$ is the gas saturation at any given time during production.

Additionally, exsolution of dissolved hydrogen from the formation water increases hydrogen availability. The exsolved gas term, $G_{EX}$, accounts for the hydrogen released from the aqueous phase:

$$G_{EX} = \frac{RT_s}{P_s}\left(n_{gi} - n_g\right) \tag{4}$$

where $R$ [J/K.mol] is the ideal gas constant, $T_s$ [K] and $P_s$ [Pa] are the temperature and pressure at surface conditions, $n_{gi}$ [mol] is the initial amount of hydrogen dissolved in the aqueous phase and $n_g$ [mol] is the remaining amount of hydrogen dissolved in the aqueous phase at any given time that can be calculated by

$$n_g = \frac{x_g n_w}{1 - x_g} \tag{5}$$

assuming that hydrogen is an ideal gas, where $x_g$ is the hydrogen mole fraction and $n_w$ [mol] is the amount of water in the aqueous phase, given by

$$n_w = \frac{(V_{wi} + W_e) \times \rho_w}{M_w} \tag{6}$$

where $V_{wi}$ [m$^3$] is the initial volume of water in the storage, $\rho_w$ [kg/m$^3$] is the water density and $M_w$ [kg/mol] is the water molar mass. With a small amount of hydrogen gas (solute) dissolved in a large volume of water (solvent), the mixture forms a dilute aqueous solution. In this case, the solute concentration is approximately proportional to its mole fraction $x_g$, which can be determined using Henry's law as:

$$x_g = \frac{P_r}{H} \tag{7}$$

where $P_r$ [Pa] is the reservoir pressure and $H$ [Pa] is the pressure dependent Henry's law constant.

The rock compressibility affects the pore space available for gas

storage. This factor, represented by $G_{RC}$, describes the gas produced because of rock expansion or contraction.

$$G_{RC} = \frac{G_i\, B_{gi}\, c_r}{S_{gi}\, B_g}\left(P_{r,i} - P_r\right) \tag{8}$$

where $c_r$ [1/Pa] is the rock compressibility.

Water compressibility also contributes to gas production as the water volume adjusts to changes in pressure, captured in the term, $G_{WC}$:

$$G_{WC} = \frac{G_i\, B_{gi}\, c_w S_{wi}}{S_{gi}\, B_g}\left(P_{r,i} - P_r\right) \tag{9}$$

where $c_w$ [1/Pa] is the water compressibility, and $S_{wi}$ is the initial water saturation.

The recovery contributions can be further classified into dimensionless indices, facilitating comparative analysis:

Gas Expansion Index:

$$I_{GE} = \frac{G_{GE}}{G_p} \tag{10}$$

Water Influx Index:

$$I_{WI} = \frac{G_{WI}}{G_p} \tag{11}$$

Exsolution Index:

$$I_{EX} = \frac{G_{EX}}{G_p} \tag{12}$$

Rock Compressibility Index:

$$I_{RC} = \frac{G_{RC}}{G_p} \tag{13}$$

Water Compressibility Index:

$$I_{WC} = \frac{G_{WC}}{G_p} \tag{14}$$

This derivation of the material balance equation for hydrogen gas production accounts for multiple reservoir parameters and processes, providing a comprehensive framework to analyse hydrogen recovery from underground storage.

## 3. Numerical simulation

We used CMG-GEM™, a compositional reservoir simulator based on the equation of state (EoS), to model the multiphase flow of hydrogen and water in UHS and to evaluate field-scale storage performance. This simulator has been used in numerous UHS simulation studies, including those referenced in Table 1. In this study, we used a sector of the PUNQ-S3 model, a 3D heterogeneous geological model based on North Sea field observations. The model was originally developed by the Elf Exploration and Production Company for oil production forecasting under uncertainty [16], but it has since been used as a test case in studies of fluid flow and mass transport for UHS and CCS [32,33,38].

The model features a central dome structure and comprises five layers of fluvial sand and shale, discretized into a grid of 19 × 28 × 5 blocks, totalling 1761 active cells with cell dimensions of 180 × 180 × 3 m [16]. For this study, we used a sector model containing only 11 × 11 × 5 grid blocks as shown in Fig. 2, to ensure an appropriate aquifer volume relative to the intended gas storage volume. Grid refinement was applied to enhance resolution, resulting in 16,335 active cells measuring 60 × 60 × 1 m each. The average formation thickness is 15 m, with an average porosity of 0.15 and an average horizontal permeability of 270 mD, and an anisotropy ratio of 0.3. Fig. 2 displays the porosity distributions in the sector model, while Table 2 summarizes the sector model parameters used in the simulation.

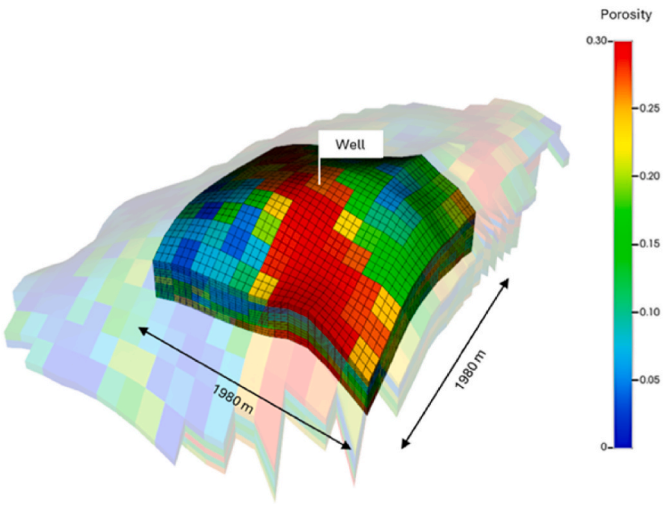



**Fig. 2.** The porosity distribution of the aquifer sector model showing the injection/production well.

**Table 2**
Sector model parameters.

| Property | Unit | Value |
|---|---|---|
| No. of active grid cells | | 16,335 |
| Discretization | m | 60 × 60 × 1 |
| Depth to surface | m | 840 |
| Thickness, $h$ | m | 15 |
| Average porosity, ∅ | | 0.15 |
| Average horizontal permeability, $k$ | mD | 270 |
| Pressure, $P$ | kPa | 9000 |
| Temperature, $T$ | C | 40 |
| Rock compressibility, $c_r$ | 1/kPa | $7.04 \times 10^{-7}$ |
| Vertical anisotropy - $K_v/K_h$ | | 0.3 |
| Total dissolved solids | | 0 % |
| Water compressibility, $c_w$ | 1/kPa | $4.07 \times 10^{-7}$ |
| Water density, $\rho_w$ | kg/m$^3$ | 992.22 |
| Water molar mass, $M_w$ | kg/mol | 0.018 |
| Water viscosity, $\mu_w$ | mPa.s | 0.653 |

Modifications to the original model included adjustments to formation depth, well location, flow rates, relative permeability, and fluid properties. These adjustments were essential to adapt the model for UHS evaluations. The top of the formation was positioned at a depth of 840 m, with initial conditions set at a pressure of 9 MPa and a temperature of 40 °C, as recommended by Ref. [38]. The single well was strategically placed at the highest structural point and perforated across the top layer of the aquifer, enabling effective hydrogen storage and withdrawal with minimum water production. The primary drainage hydrogen-water relative permeability obtained from Ref. [17] in Fig. 3 was used. For gas hysteresis, the maximum residual gas saturation after imbibition was used to calculate the Land trapping parameter that is needed for the Carlson hysteresis model [39]. Capillary pressure effects can typically be neglected when numerically simulating field-scale displacements [38].

For fluid properties, the Peng-Robinson EOS [37] was used to estimate the phase behaviour between hydrogen and water, with CMG-WinProp quantifying phase-equilibrium compositions and thermodynamic properties. Henry's Law, Eq. (7) [40] was used to model the solubility of hydrogen in water. The density and viscosity of the cushion gas were determined using correlations from Jossi (1965) [41] and Peng-Robinson (1976) [37], respectively. The aquifer was initially saturated with water, and its properties were obtained from the literature as detailed in Table 2.

Two base scenarios were considered: Case A - closed boundary conditions with no active aquifer support, and Case B - open boundary conditions with water influx from a well-connected aquifer. In each

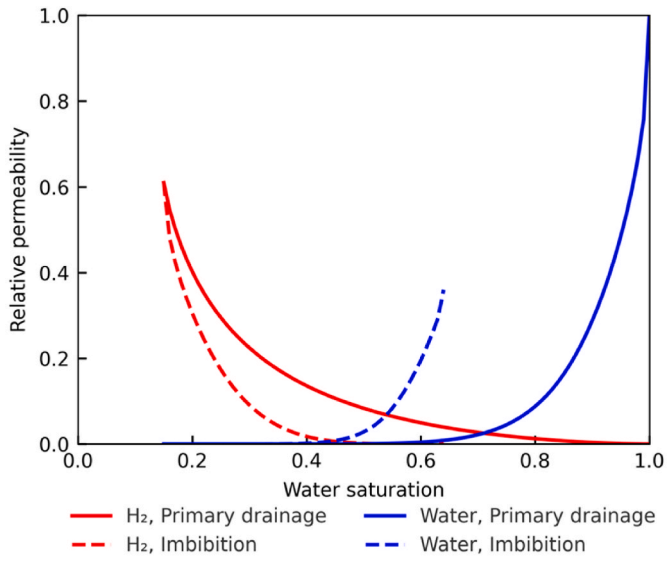



**Fig. 3.** Primary drainage and imbibition relative permeabilities for hydrogen-water obtained from Ref. [17].

scenario, five injection-withdrawal cycles were performed. Each cycle involved using the well for both injecting and withdrawing hydrogen at a rate of 200,000 $sm^3$/day. Hydrogen was injected into the aquifer for six months, followed by a six-month withdrawal period. The well operated under minimum wellhead pressure of 5 MPa during withdrawal. The production well had a diameter of 0.1524 m, and a skin factor of zero was applied, indicating no alterations to the formation properties around the wellbore. To simulate aquifer support in Case B, the sector model was linked to a bottom-drive, infinite-acting aquifer, modelled using the Carter-Tracy analytical approach [13]. Table 3 presents the operational parameters and Table 4 shows a summary of the simulation scenarios considered.

## 4. Results and discussion

Fig. 4 shows the hydrogen distributions, comparing Case A (no active aquifer) and Case B (infinite-acting aquifer) over five injection-withdrawal cycles. Although the amount of dissolved hydrogen is very low due to hydrogen's low solubility, it increased steadily with each cycle in both cases. The presence of an infinite-acting aquifer support in Case B did not significantly alter the amount of hydrogen that dissolved compared to Case A. The residually trapped and mobile gas represents the hydrogen that remained in the reservoir as a free gas phase. At the end of each production cycle, Case B showed a higher volume of free gas, suggesting that the stable pressure maintained by the aquifer leads to less effective displacement of hydrogen towards production wells, thus retaining more hydrogen within the reservoir (the hydrogen is at a higher pressure and hence has a larger density). Conversely, Case A exhibited lower volumes of free gas, due to more significant pressure reductions enhancing hydrogen migration toward production wells. Additionally, in Case A, the aquifer water remains confined within the storage zone during hydrogen injection. This causes the injected hydrogen to compress, occupying less pore volume compared to the aquifer water. This effect is clearly illustrated in Fig. 5, which shows the spatial extent of the hydrogen plume across the aquifer at the start of the production cycles. Therefore, Case A and its variants exhibit significantly higher water-to-gas ratios than Case B and its variants in the underground storage as illustrated in Fig. 6. In this study, this design was purposefully used to study drive mechanism contributions in these two extreme scenarios.

**Table 3**
Operational parameters for all simulation scenarios.

| Parameter | Unit | Value |
|---|---|---|
| Working gas (WG) | | $H_2$ |
| Injection & production rate | $sm^3$/day | 200,000 |
| Production well diameter | m | 0.1524 |
| Skin factor | | 0 |
| Min well-head pressure | kPa | 5000 |
| Injection period per cycle | Days | 183 |
| Production period per cycle | Days | 182 |

Fig. 7 illustrates gas recovery across all the scenarios presented in Table 4. Recovery generally improves or stabilizes over time, though early cycles exhibit significant variability, highlighting differing initial efficiencies. Case A5 and Case B5 with no hysteresis consistently outperform other cases. The impact of cyclic operations on storage performance are clearly demonstrated in the simulation results. Consequently, the analysis focuses on both the 1st and 5th production cycles to better understand the various drive mechanisms.

Fig. 8 shows the cumulative hydrogen production, $G_p^{sim}$, as directly determined from the simulator and the calculated $G_p^{mbe}$ from material balance Eq. (1) considering the various drive mechanisms. The simulation data used for the calculation included initial gas and water volumes, gas formation volume factor, average saturation, average pressure, and model parameters listed in Table 2. The maximum percentage errors observed between $G_p^{sim}$ and $G_p^{mbe}$ were 5.4 % for Case A and 5.7 % for Case B, indicating a high level of reliability in using the material balance approach, which assumes averaged properties, to calculate the dimensionless drive indices.

### 4.1. Closed boundary conditions

Case A serves as a benchmark for comparing other simulation scenarios, providing insights into the fundamental drive mechanisms under typical storage conditions without active aquifer support. This case includes the effects of solubility, compressibility, and hysteresis. Fig. 9 presents the simulation results for Case A and its variations (A1–A5 as described in Table 4), including the calculated drive mechanism contribution indices (Eqs. (10)–(14)) and the corresponding pressure trends as a function of cumulative gas production. The pressure trends indicate a steady decline in Case A, reflecting depletion-driven behaviour where pressure support is governed by internal processes within the storage formation.

- Gas Expansion: The gas expansion contribution denoted $I_{GE}$ remains stable and consistently dominant across both the 1st and the 5th production cycles. This stability indicates that the expansion of hydrogen gas due to changes in pressure is the main driving force for production. The nearly unchanged pattern between the 1st and 5th cycles suggests that the system reaches a stable state relatively quickly, where the dynamics of gas expansion are well-established and predictable. This behaviour is crucial for ensuring reliable hydrogen output over multiple production cycles.
- Gas Exsolution: The contribution from gas exsolution $I_{EX}$ is negligible throughout both cycles. This observation implies that under base conditions, there is little to no phase separation occurring where hydrogen gas would be released from a dissolved state in the formation water. The absence of significant gas exsolution can be also attributed to the relatively small amount of hydrogen dissolved in the water as shown in Fig. 4(a). This simplifies the dynamics of gas storage and reduces the complexity of predicting gas behaviour based on phase changes.
- Rock Compressibility: The initial increase in the rock compressibility index $I_{RC}$ suggests that the rock within the formation has some capacity to compress under pressure changes: the porosity increases with fluid pressure during injection and decreases during production. Although this effect quickly stabilizes indicating that any

**Table 4**
A summary of simulation scenarios.

| Case | A (Base) | A1 | A2 | A3 | A4 | A5 | B (Base) | B1 | B2 | B3 | B4 | B5 |
|---|---|---|---|---|---|---|---|---|---|---|---|---|
| Aquifer support | | | | | | | ✓ | ✓ | ✓ | ✓ | ✓ | ✓ |
| Solubility | ✓ | | ✓ | ✓ | | ✓ | ✓ | | ✓ | ✓ | | ✓ |
| High $c_r$ | | | ✓ | | | | | | ✓ | | | |
| Cushion gas | | | | $H_2$ | $CH_4$ | | | | | $H_2$ | $CH_4$ | |
| Hysteresis | ✓ | ✓ | ✓ | ✓ | ✓ | | ✓ | ✓ | ✓ | ✓ | ✓ | |

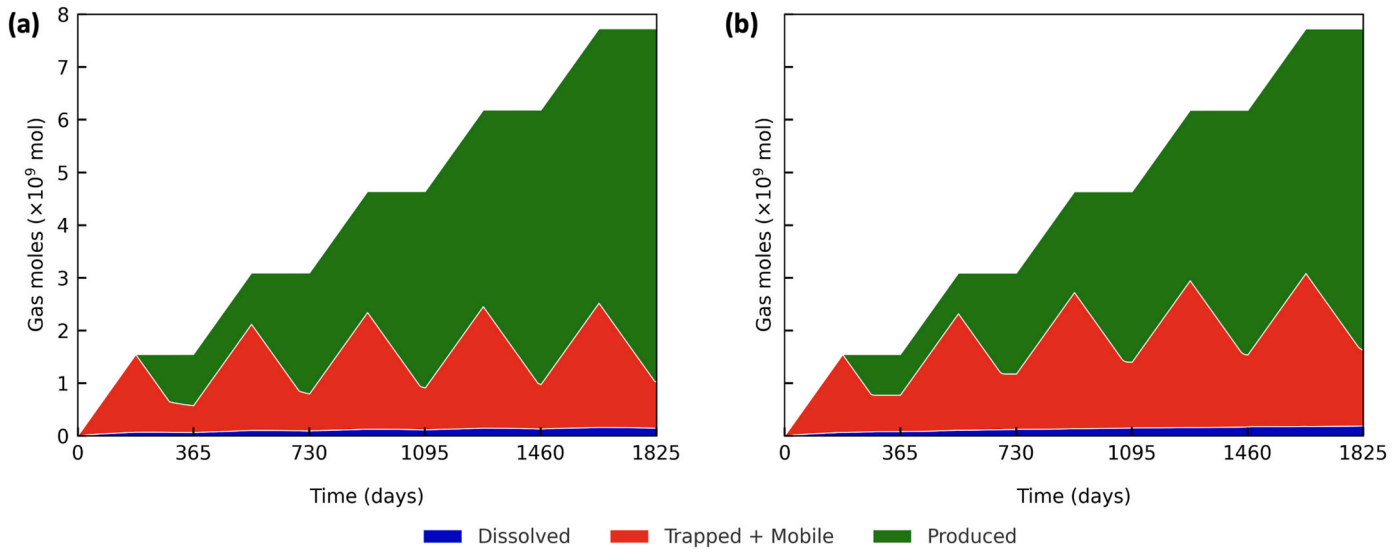



**Fig. 4.** Hydrogen distribution across different phases over five injection/production cycles: (a) Case A – closed boundary conditions without aquifer support; (b) Case B – open boundary conditions with infinite-acting aquifer support.

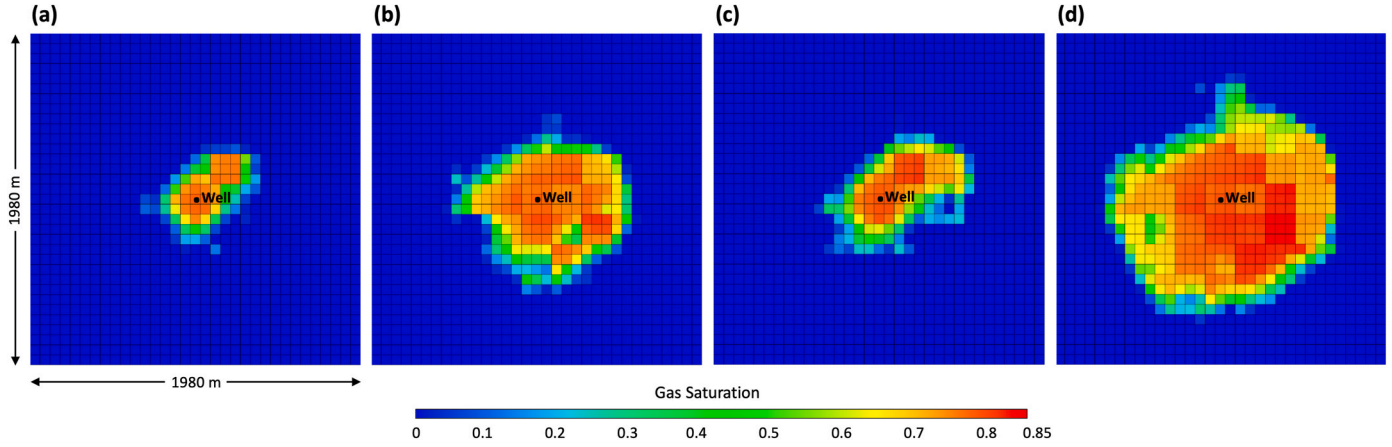



**Fig. 5.** 2D maps of gas saturation illustrating the spatial extent of the hydrogen plume across the aquifer: (a) Case A and (b) Case B at the start of the 1st production cycle; (c) Case A and (d) Case B at the start of the 5th production cycle.

deformation of the rock matrix is limited, it significantly contributes to the overall gas recovery under closed boundary conditions with a magnitude similar to the gas expansion effect.

- Water Compressibility: $I_{WC}$ shows almost no deviation across the cycles, indicating that the low water compressibility has less contribution to hydrogen recovery in this scenario. This stability suggests that formation water within the reservoir has little impact on the behaviour.

Overall, Case A establishes a baseline understanding where gas expansion and rock compressibility are the critical drivers for hydrogen recovery under closed boundary conditions, with the other mechanisms, gas exsolution and water compressibility playing minimal roles. In Case A1, A2, A3, A4 and A5, the sensitivity to different processes and parameters are investigated.

In Case A1, since it considers a scenario with no solubility, there is no gas exsolution as shown in Fig. 9(b). This allows more of the injected hydrogen to remain in the free gas phase, further increasing the volume of gas available to expand as pressure declines during production, as observed in the first cycle. In contrast, when solubility is present (Case A), a portion of the hydrogen dissolves into the formation water, reducing the initial free gas volume. This lowers the gas expansion potential since only the free gas phase contributes directly to this mechanism. As a result, $I_{GE}$ continues to be the primary driving force. Both $I_{RC}$

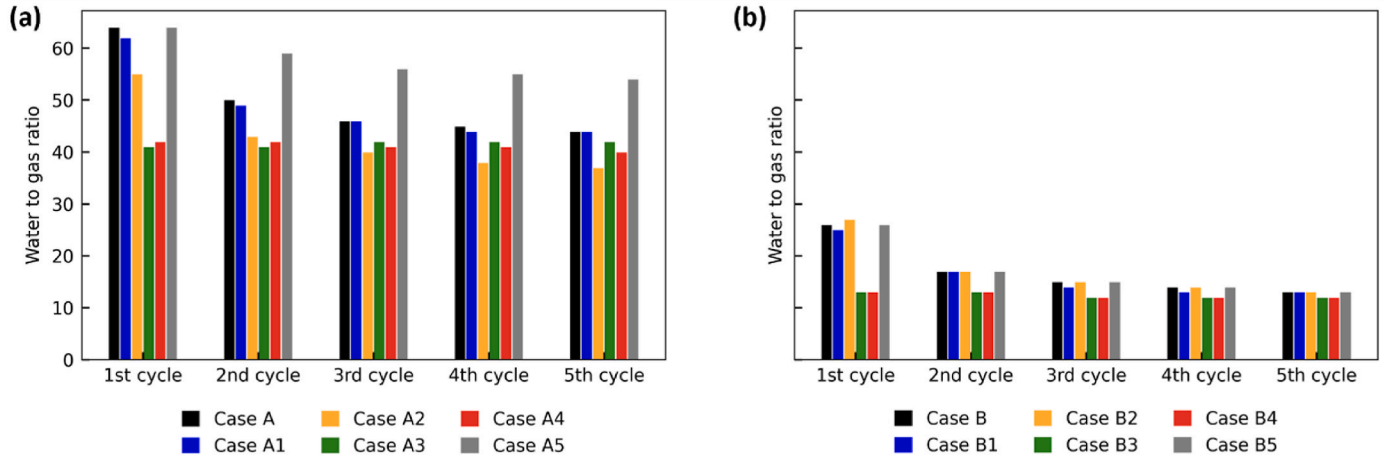



**Fig. 6.** Water-to-gas ratio at the start of each production cycle: (a) Closed boundary conditions without aquifer support; (b) Open boundary conditions with infinite-acting aquifer support.

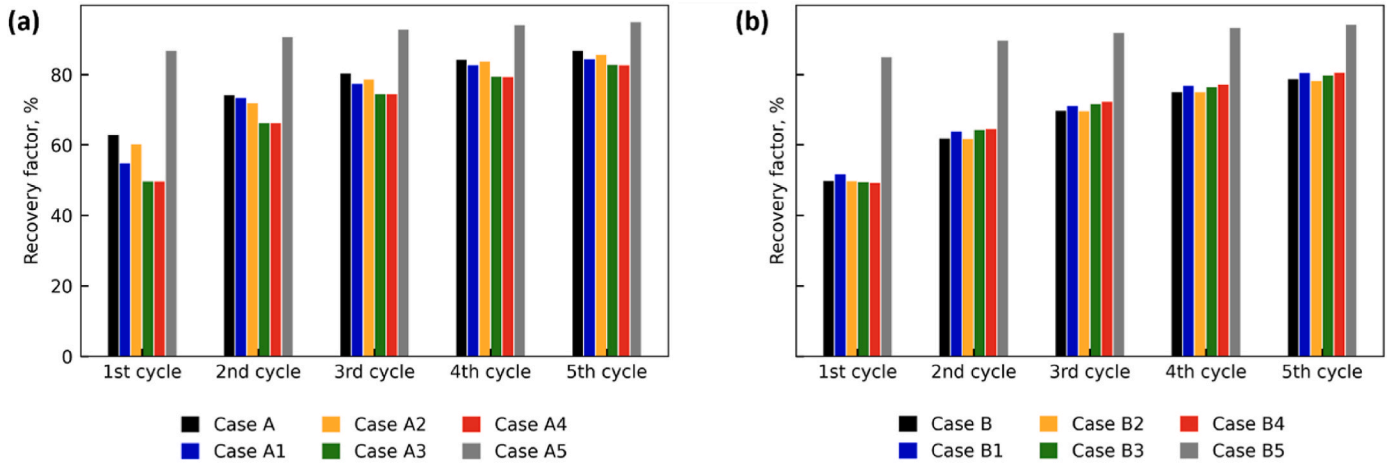



**Fig. 7.** Gas recovery at the end of each production cycle: (a) Closed boundary conditions without aquifer support; (b) Open boundary conditions with infinite-acting aquifer support.

and $I_{WC}$ contribute similarly to the base scenario, confirming that the lack of solubility primarily affects gas exsolution and, to a lesser extent, gas expansion, without significantly impacting other mechanisms.

Case A2, characterized by high rock compressibility of $1.408 \times 10^{-9}$ 1/Pa, shows a marked increase in $I_{RC}$, especially noticeable in the initial days as shown in Fig. 9(c). This indicates that the storage capacity and dynamics are significantly influenced by the rock's physical response to pressure changes. The behaviours of $I_{GE}$ and $I_{EX}$ are similar to those in Case A, with no significant changes. However, $I_{WC}$ slightly decreased.

Case A3 highlighted the effects of initial cushion gas injection. Cushion gas is often used to maintain pressure, ensure operational integrity, and prevent hydrogen from being trapped by water encroachment [1,2]. In Case A3, hydrogen was used as a cushion gas to reduce gas mixing effects. Extended production periods in early cycles were observed due to the increased amount of mobile gas available for production. In terms of recovery contributions, no significant changes were observed as shown in Fig. 9(d).

In Case A4, methane ($CH_4$) was used as cushion gas. The solubility of both hydrogen and methane in water was disregarded in this case, as previous scenarios showed that hydrogen exsolution had a negligible effect on overall recovery. While methane is slightly more soluble than hydrogen, both gases have low solubility in water under the conditions considered [15,42]. This simplification allows the analysis to focus on gas-phase mechanisms. Similar to Case A3, extended production periods in the early cycles were observed due to the increased amount of mobile gas available for production. Fig. 9(e) shows a slight decrease in $I_{GE}$, which could be attributed to the lower compressibility of $CH_4$. In practical terms, hydrogen, owing to its lower molecular weight and higher compressibility, expands more significantly than a mixture of hydrogen and methane when subjected to decreasing pressure. The expansion of the gas mixture is less pronounced than that of pure hydrogen but greater than that of pure methane under the same conditions observed in Case A3. Regarding other drive mechanisms, no significant changes were observed.

In Case A5, the hysteresis effect was removed, allowing all residually trapped gas to become mobile and be produced. We observed a more efficient response to pressure changes that enhanced overall gas recovery, especially in the early cycles. Fig. 9(f) shows that Case A5 exhibits behaviours similar to that of $I_{GE}$, $I_{RC}$, $I_{WC}$, and $I_{EX}$ in Case A.

Across different scenarios, the analysis consistently identifies gas expansion as the primary and most stable drive mechanism within UHS, exerting significant influence across all cases. Additionally, the type of cushion gas used has a slight impact on the expansion process. Under closed boundary conditions with no aquifer support, rock compressibility plays a crucial role in hydrogen recovery, where high compressibility markedly affects storage dynamics. The contributions of gas

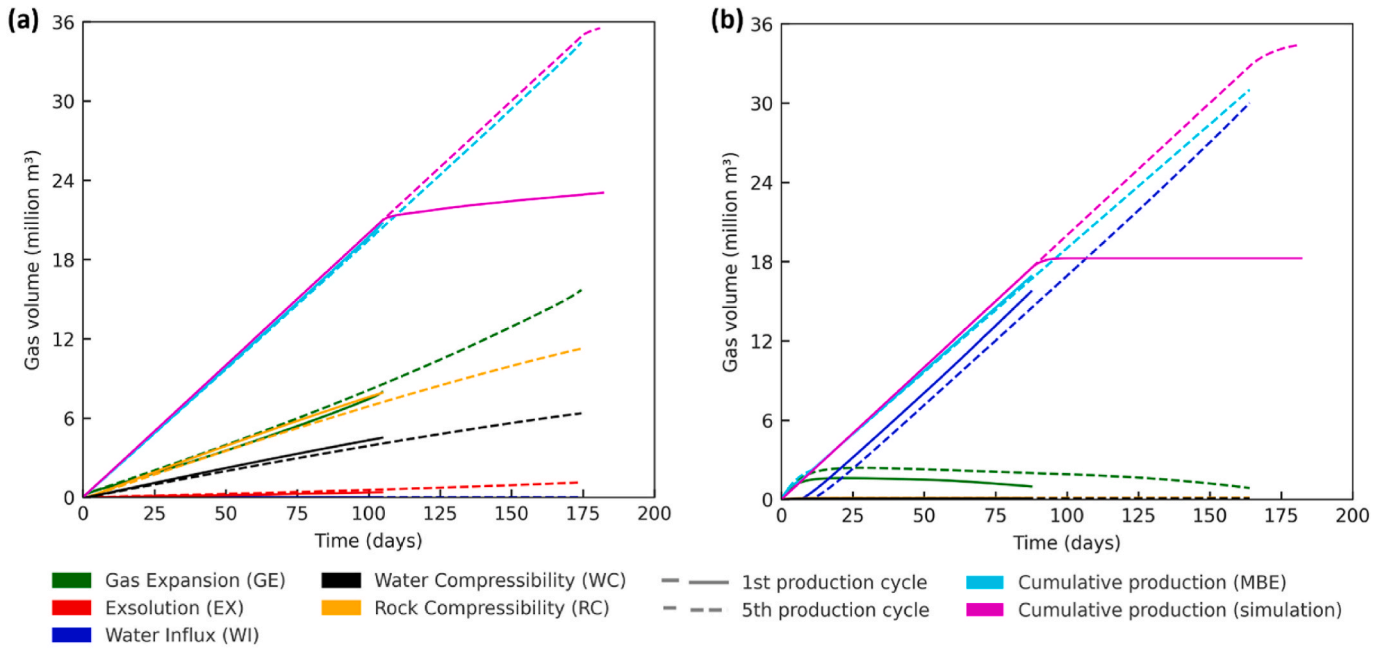



**Fig. 8.** Cumulative hydrogen production from numerical simulation and material balance, along with the relative contribution of each drive mechanism: (a) Case A – closed boundary conditions without aquifer support; (b) Case B – open boundary conditions with infinite-acting aquifer support.

exsolution and water compressibility are notably minor in all the scenarios considered, underscoring their limited influence under the conditions studied.

This analysis suggests that in assessing hydrogen storage in closed reservoirs, the most important parameters to measure are gas and rock compressibility. In particular, it is necessary to have an accurate understanding of the response of the formation to pressure fluctuations, including hysteresis in mechanical properties and the fracture pressure, which lies beyond the scope of the work presented here.

### 4.2. Open boundary conditions

Fig. 10 presents the results for Case B and its variations (B1–B5), showing the relative contribution indices of each drive mechanism alongside the corresponding pressure trends as a function of cumulative gas production. In Case B, pressure remains high across cycles, indicating minimal depletion due to strong aquifer support, unlike the depletion-driven behaviour observed in Case A. The dominant processes differ significantly between the two cases, particularly due to the influence of external factors acting on the storage formation. Fig. 10(a) shows how each mechanism contributes to hydrogen recovery in Case B.

- Gas Expansion: Unlike Case A, where gas expansion was a significant driver, this mechanism plays a more limited role in Case B. Despite the initial gas volume being the same, the reduced impact of gas expansion is due to a limited pressure decline, which does not support substantial expansion of hydrogen. Over time, this results in minimal contributions from $I_{GE}$, indicating a reliance on the displacement of hydrogen by incoming water rather than its expansion.
- Water Influx: $I_{WI}$ emerges as the dominant factor in Case B, with a steep increase early in the 1st cycle and to a lesser extent in the 5th cycles. This pronounced effect suggests that the geological setting such as the strong connectivity of the reservoir to surrounding water-bearing formations, significantly facilitates water movement into the storage zone. The steep rise indicates a high hydraulic gradient that drives water into the reservoir, compensating for the pressure drop as hydrogen is withdrawn. As the cycle progress, this influx starts to stabilize due to the equalization of pressure differentials between the storage zone and the adjacent aquifer.
- Rock and Water Compressibility: $I_{RC}$ and $I_{WC}$ show negligible effects throughout the cycles. With the properties of the rock and water remaining the same as in Case A, this minimal impact suggests that the changes in pressure do not significantly alter their volumes. This stability is advantageous for maintaining the structural integrity of the reservoir but also indicates that these factors do not aid in hydrogen recovery under the current conditions.
- Gas Exsolution: there is no significant gas exsolution. Although the amount of hydrogen dissolved is similar to Case A, the limited pressure fluctuation prevents hydrogen from being released from water. The absence of $I_{EX}$ simplifies the dynamics within the storage.

Overall, Case B indicates a scenario where the effect of hydraulic factors overrides the effect of thermodynamic properties of hydrogen, leading to a drive mechanism primarily influenced by water movement rather than gas dynamics. In Case B1, B2, B3 and B4, the sensitivity to different processes and parameters are investigated.

Case B1, characterized by an absence of hydrogen solubility, shows behaviour similar to the base scenario as shown in Fig. 10(b). The improvement in $I_{GE}$ over time is attributed to the larger volume of hydrogen available in free gas phase compared to the base scenario. Despite this, $I_{WI}$ remains the dominant drive mechanism. $I_{RC}$ and $I_{WC}$ are negligible. This consistency across cases where solubility is altered suggests that the storage dynamics are more influenced by physical rather than chemical properties of the system.

The high rock compressibility scenario (Case B2) highlights the rock's capacity to compress under pressure, evidenced by a pronounced $I_{RC}$, particularly in the early phase across cycles as shown in Fig. 10(c). This suggests that the additional pore space created by rock deformation may temporarily enhance storage capacity but quickly stabilizes, affecting storage dynamics only initially. Other mechanisms follow patterns similar to Case B.

Case B3 and Case B4 showcase the effectiveness of cushion gas injection in enhancing the contribution of gas expansion by increasing the free gas phase available in the storage, especially in the early cycles as shown in Fig. 10(d and e). This also leads to an increase in recovery by

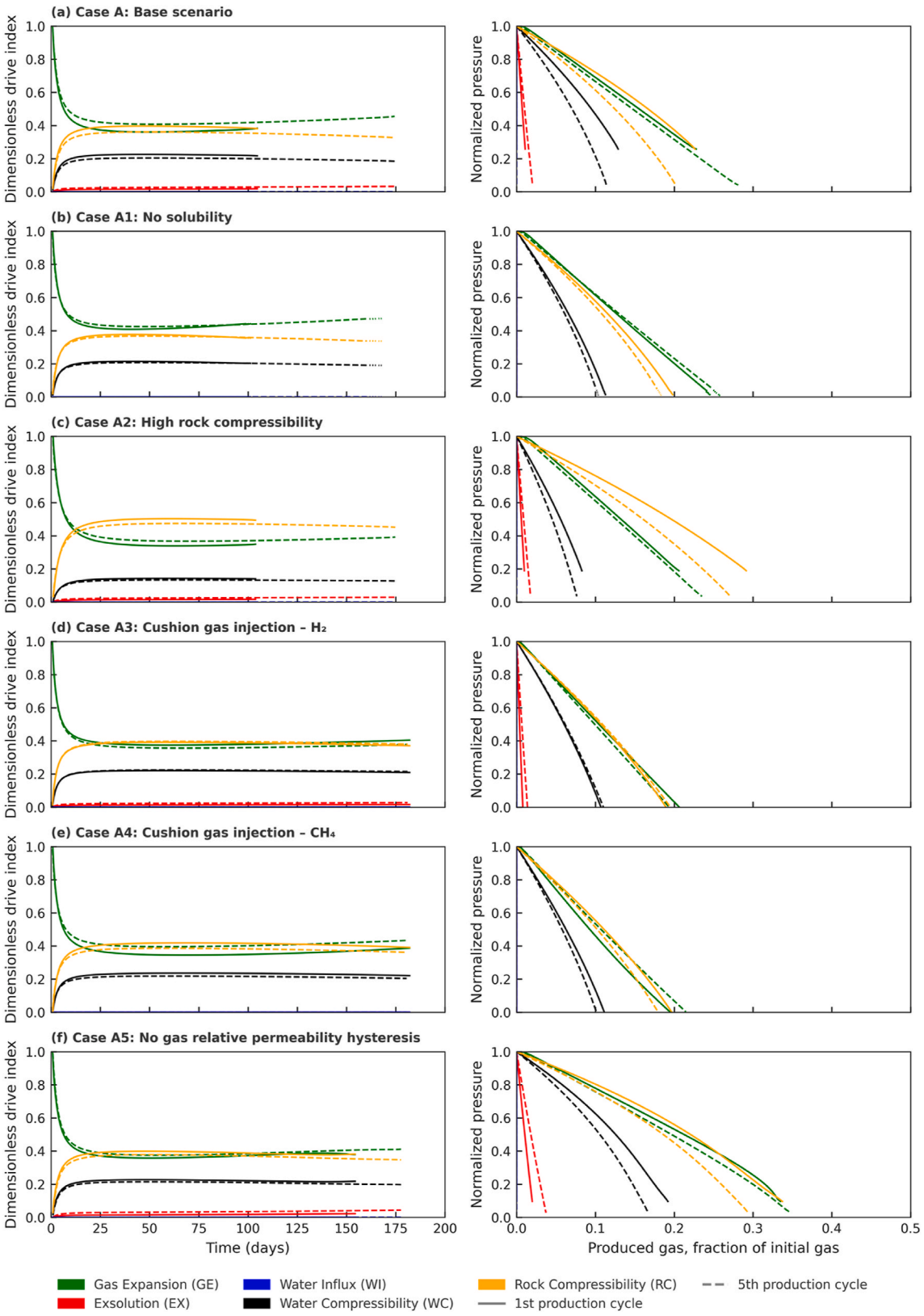



**Fig. 9.** Drive mechanism indices and normalized pressure per cycle versus produced gas under closed boundary conditions for the 1st and 5th production cycles: (a) base case, (b) no solubility, (c) high rock compressibility, (d) (e) cushion gas injection with $H_2$ and $CH_4$ respectively, and (f) no hysteresis (trapping).

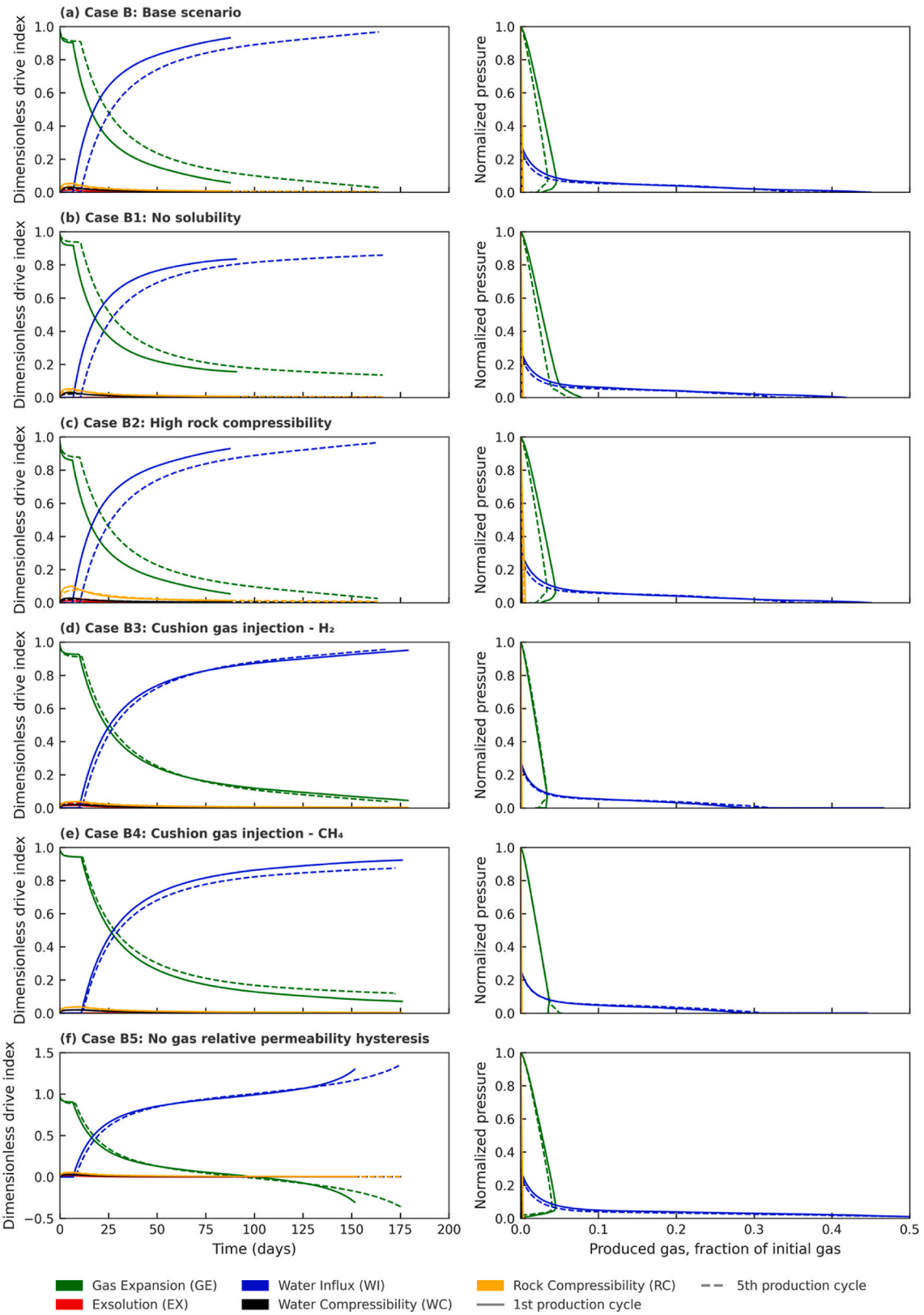



**Fig. 10.** Drive mechanism indices and normalized pressure per cycle versus produced gas under open boundary conditions for the 1st and 5th production cycles: (a) base case, (b) no solubility, (c) high rock compressibility, (d) (e) cushion gas injection with $H_2$ and $CH_4$ respectively, and (f) no hysteresis (trapping).

extending the production period. Nevertheless, $I_{WI}$ remains the dominant drive mechanism over time as pressure declines. $I_{RC}$, $I_{WC}$, along with $I_{EX}$, remain minimal. Case B3 and Case B4 demonstrate the role of cushion gas in enhancing gas recovery and highlight the added benefit of using a more compressible gas, such as hydrogen, in further increasing the contribution of gas expansion.

In Case B5 (no hysteresis), key distinctions are observed in the behaviour of gas expansion and water influx, both of which exhibit more rapid and pronounced responses near the end of each production cycle. The calculated drive indices $I_{WI}$ and $I_{GE}$ fall outside the range of 0–1, as shown in Fig. 10(f). Both simulation and material balance results display similar patterns of water influx, suggesting an increase in water entering the storage domain. This appears to prevent gas expansion and instead compresses the gas. This indicates that the absence of hysteresis facilitates immediate pressure adjustments from the infinite-acting aquifer. Conversely, $I_{RC}$, $I_{WC}$, along with $I_{EX}$ remain unaffected by the presence or absence of hysteresis.

Across the different scenarios in Case B, water influx emerges as the primary drive mechanism, highlighting its critical role under specific geological and operational conditions. The scenarios also demonstrate that uncertainty regarding rock compressibility has little influence on the dominant drive mechanism, unlike in Case A. However, operational strategies such as cushion gas injection prove to be effective in enhancing gas expansion. This strategy streamlines the storage process in early cycles by reducing reliance on less controllable mechanisms, such as water influx and rock compressibility.

The key consideration in a case with an active aquifer drive is the degree of relative permeability hysteresis and capillary trapping with multiple cycles of injection and withdrawal. This is a likely a major uncertainty: a careful assessment of residual gas saturation is required to manage the field appropriately. This requires a quantification of the behaviour for continuous injection and withdrawal cycles that includes the effect of transport of gas in the aqueous phase to rearrange the gas in the pore space, leading to reduced trapping [43].

## 5. Conclusions

We evaluated the drive mechanisms contributing to hydrogen recovery in UHS through numerical simulations in a putative storage facility interpreted using material balance analysis. The study analysed both closed and open boundary conditions. Our analysis provides the following insights into the dynamics of hydrogen storage.

- For closed boundary conditions, gas expansion and rock compressibility are the predominant mechanisms driving hydrogen recovery. These mechanisms are always the most significant, followed by water compressibility.
- Water influx, which is controlled by geological connectivity and hydraulic gradients, emerges as the primary driver of hydrogen recovery with open boundary conditions.
- Exsolution has minimal influence on hydrogen recovery under both open and closed boundary conditions, thereby simplifying the predictive modelling of storage dynamics.
- Cushion gas injection has been observed to enhance gas expansion, particularly critical in open boundary scenarios, optimizing hydrogen recovery during initial production cycles.

This work provides a framework for quantifying the mechanisms responsible for hydrogen production that can be applied to proposed storage projects. It also identifies the key uncertainties and properties that need to be measured to obtain accurate predictions of performance. In cases with no active aquifer, rock compressibility controls the pressure response in the formation. This property must be accurately assessed, and formations with high compressibility are preferred, as highlighted in Case A2, where rock compressibility significantly influenced pressure support and recovery, as evidenced by the increased contribution of the rock compressibility index. In contrast, if an active aquifer is present, compressibility becomes less important. Instead, relative permeability characteristics, such as trapping and hysteresis across multiple injection and withdrawal cycles, control the behaviour. As seen in Case B5, the removal of hysteresis altered the pressure response, leading to gas compression rather than expansion due to the rapid influx of water from the aquifer. Accurate characterisation of fluid and rock properties under representative conditions is essential for effective storage management.

These findings also support practical decision-making for UHS planning. For example, identifying whether a storage setting behaves under closed or open boundary conditions can inform whether to prioritize rock compressibility or multiphase flow properties in site assessment. Cushion gas strategies, particularly using hydrogen, offer a controllable way to enhance early-cycle recovery. Tailoring injection and withdrawal strategies to match dominant drive mechanisms can improve both performance and predictability.

Future work should focus on applying this material balance methodology to proposed field sites, as well as inputting multiphase flow characteristics measured under conditions of both displacement and pressure increase and decline [12]. These conditions are distinct from those traditionally imposed for flow measurements for oilfield applications and may require a different formulation for relative permeability and capillary pressure, including trapping and hysteresis.

## CRediT authorship contribution statement

**Ibrahim A. Alobaidan:** Writing – original draft, Visualization, Software, Methodology, Investigation, Formal analysis, Data curation, Conceptualization. **Branko Bijeljic:** Writing – review & editing, Supervision, Conceptualization. **Martin J. Blunt:** Writing – review & editing, Validation, Supervision, Methodology, Conceptualization.

## Declaration of competing interest

The authors declare that they have no known competing financial interests or personal relationships that could have appeared to influence the work reported in this paper.

## Acknowledgments

We thank Saudi Aramco for their support through a PhD sponsorship.

## Nomenclature

| Symbol | Description |
|---|---|
| $G_p$ | Gas produced from the storage at surface conditions, $m^3$ |
| $G_i$ | Initial free gas in place before production at surface conditions, $m^3$ |
| $B_g$ | Gas formation volume factor |
| $P$ | Average reservoir pressure, Pa |

(*continued on next page*)

(*continued*)

| Symbol | Description |
|---|---|
| $T$ | Reservoir temperature, K |
| $S_g$ | Gas saturation |
| $S_w$ | Water saturation |
| $c_r$ | Rock compressibility, 1/Pa |
| $c_w$ | Water compressibility, 1/Pa |
| $\rho_w$ | Water density, kg/m$^3$ |
| $M_w$ | Water molar mass, kg/mol |
| $Z$ | Mole fraction of free hydrogen gas in reservoir |
| $V_{wi}$ | Initial volume of water in the reservoir, m$^3$ |
| $H$ | Pressure-dependent Henry's law constant |

## References


[1] Hematpur H, Abdollahi R, Rostami S, Haghighi M, Blunt MJ. Review of underground hydrogen storage: concepts and challenges. In: Advances in geo-energy research, 7. Yandy Scientific Press; 2023. p. 111–31.

[2] Lord AS, Kobos PH, Borns DJ. Geologic storage of hydrogen: scaling up to meet city transportation demands. Int J Hydrogen Energy 2014;39(28):15570–82. https://doi.org/10.1016/j.ijhydene.2014.07.121.

[3] Tarkowski R. Underground hydrogen storage: characteristics and prospects. In: Renewable and sustainable energy reviews, 105. Elsevier Ltd; 2019. p. 86–94.

[4] Heinemann N, et al. Enabling large-scale hydrogen storage in porous media-the scientific challenges. In: Energy and environmental science, 14. Royal Society of Chemistry; 2021. p. 853–64.

[5] Paterson L. The implications of fingering in underground hydrogen storage. Int J Hydrogen Energy 1983;8(1):53–9. https://doi.org/10.1016/0360-3199(83)90035-6.

[6] Tek MR, N. A. T. O. S. A. Division. Underground storage of natural gas: theory and practice. Netherlands: Springer; 1989.

[7] Feldmann F, Hagemann B, Ganzer L, Panfilov M. Numerical simulation of hydrodynamic and gas mixing processes in underground hydrogen storages. Environ Earth Sci 2016;75(16). https://doi.org/10.1007/s12665-016-5948-z.

[8] Zhao Q, Wang Y, Chen C. Numerical simulation of the impact of different cushion gases on underground hydrogen storage in aquifers based on an experimentally-benchmarked equation-of-state. Int J Hydrogen Energy 2023. https://doi.org/10.1016/j.ijhydene.2023.07.262.

[9] Blunt MJ. Multiphase flow in permeable media: a pore-scale perspective. Cambridge: Cambridge University Press; 2017.

[10] Ahmed T, McKinney P. Advanced reservoir engineering. Gulf Professional Publishing; 2011.

[11] Dake LP. Fundamentals of reservoir engineering. Amsterdam: Elsevier; 1978.

[12] Dokhon W, Goodarzi S, Alzahrani HM, Blunt MJ, Bijeljic B. Pressure decline and gas expansion in underground hydrogen storage: a pore-scale percolation study. Int J Hydrogen Energy 2024;86:261–74. https://doi.org/10.1016/j.ijhydene.2024.08.139.

[13] Carter RD, Tracy GW. An improved method for calculating water influx. Trans AIME 1960;219(1):415–7. https://doi.org/10.2118/1626-g.

[14] Fetkovich MJ. A simplified approach to water influx calculations-finite aquifer systems. J Petrol Technol 1971;23(7):814–28. https://doi.org/10.2118/2603-pa.

[15] Chabab S, Théveneau P, Coquelet C, Corvisier J, Paricaud P. Measurements and predictive models of high-pressure H2 solubility in brine (H2O+ NaCl) for underground hydrogen storage application. Int J Hydrogen Energy 2020;45(56):32206–20. https://doi.org/10.1016/j.ijhydene.2020.08.192.

[16] Floris F, Bush M, Cuypers M, Roggero F, Syversveen A. Methods for quantifying the uncertainty of production forecasts: a comparative study. Pet Geosci 2001;7. https://doi.org/10.1144/petgeo.7.S.S87.

[17] Lysyy M, Føyen T, Johannesen EB, Fernø M, Ersland G. Hydrogen relative permeability hysteresis in underground storage. Geophys Res Lett 2022;49(17). https://doi.org/10.1029/2022GL100364.

[18] Heinemann N, et al. Hydrogen storage in saline aquifers: the role of cushion gas for injection and production. Int J Hydrogen Energy 2021;46(79):39284–96. https://doi.org/10.1016/j.ijhydene.2021.09.174.

[19] Yekta AE, Manceau JC, Gaboreau S, Pichavant M, Audigane P. Determination of hydrogen–water relative permeability and capillary pressure in sandstone: application to underground hydrogen injection in sedimentary formations. Transport Porous Media 2018;122(2):333–56. https://doi.org/10.1007/s11242-018-1004-7.

[20] Okoroafor ER, Saltzer SD, Kovscek AR. Toward underground hydrogen storage in porous media: reservoir engineering insights. Int J Hydrogen Energy 2022;47(79):33781–802. https://doi.org/10.1016/j.ijhydene.2022.07.239.

[21] Kanaani M, Sedaee B, Asadian-Pakfar M. Role of cushion gas on underground hydrogen storage in depleted oil reservoirs. J Energy Storage 2022;45. https://doi.org/10.1016/j.est.2021.103783.

[22] Delshad M, Umurzakov Y, Sepehrnoori K, Eichhubl P, Batista Fernandes BR. Hydrogen storage assessment in depleted oil reservoir and saline aquifer. Energies 2022;15(21). https://doi.org/10.3390/en15218132.

[23] Huang T, Moridis GJ, Blasingame TA, Abdulkader AM, Yan B. Compositional reservoir simulation of underground hydrogen storage in depleted gas reservoirs. Int J Hydrogen Energy 2023. https://doi.org/10.1016/j.ijhydene.2023.05.355.

[24] Stone HL. Probability model for estimating three-phase relative permeability. J Petrol Technol 1970;22(2):214–8. https://doi.org/10.2118/2116-pa.

[25] Jadhawar P, Saeed M. Optimizing the operational efficiency of the underground hydrogen storage scheme in a deep North Sea aquifer through compositional simulations. J Energy Storage 2023;73. https://doi.org/10.1016/j.est.2023.108832. 108832-108832.

[26] Bahrami M, Izadi Amiri E, Zivar D, Ayatollahi S, Mahani H. Challenges in the simulation of underground hydrogen storage: a review of relative permeability and hysteresis in hydrogen-water system. Journal of energy storage, 73. Elsevier Ltd; 2023.

[27] Pfeiffer WT, al Hagrey SA, Köhn D, Rabbel W, Bauer S. Porous media hydrogen storage at a synthetic, heterogeneous field site: numerical simulation of storage operation and geophysical monitoring. Environ Earth Sci 2016;75(16):1177. https://doi.org/10.1007/s12665-016-5958-x.

[28] Kunz O, Wagner W. The GERG-2008 wide-range equation of state for natural gases and other mixtures: an expansion of GERG-2004. J Chem Eng Data 2012;57(11):3032–91. https://doi.org/10.1021/je300655b.

[29] Lysyy M, Fernø MA, Ersland G. Effect of relative permeability hysteresis on reservoir simulation of underground hydrogen storage in an offshore aquifer. J Energy Storage 2023;64. https://doi.org/10.1016/j.est.2023.107229.

[30] Bo Z, Boon M, Hajibeygi H, Hurter S. Impact of experimentally measured relative permeability hysteresis on reservoir-scale performance of underground hydrogen storage (UHS). Int J Hydrogen Energy 2023;48(36):13527–42. https://doi.org/10.1016/j.ijhydene.2022.12.270.

[31] Boon M, Hajibeygi H. Experimental characterization of H2/water multiphase flow in heterogeneous sandstone rock at the core scale relevant for underground hydrogen storage (UHS). Sci Rep 2022;12(1):14604. https://doi.org/10.1038/s41598-022-18759-8.

[32] Ershadnia R, et al. Impact of geological and operational conditions on underground hydrogen storage. Int J Hydrogen Energy 2023;48(4):1450–71. https://doi.org/10.1016/j.ijhydene.2022.09.208.

[33] Pan B, et al. Impacts of relative permeability hysteresis, wettability, and injection/withdrawal schemes on underground hydrogen storage in saline aquifers. Fuel 2023;333. https://doi.org/10.1016/j.fuel.2022.126516.

[34] Saeed M, Jadhawar P. Optimizing underground hydrogen storage in aquifers: the impact of cushion gas type. Int J Hydrogen Energy 2024;52:1537–49. https://doi.org/10.1016/j.ijhydene.2023.08.352.

[35] Kumbhat DS, Ebigbo A. Effect of relative permeability hysteresis on plume dynamics, wellbore flow regime, and storage efficiency in underground hydrogen storage. Int J Hydrogen Energy 2024;91:243–55. https://doi.org/10.1016/j.ijhydene.2024.09.403.

[36] Soave G. Equilibrium constants from a modified Redlich-Kwong equation of state. Chem Eng Sci 1972;27(6):1197–203. https://doi.org/10.1016/0009-2509(72)80096-4.

[37] Peng D-y, Robinson D. New two-constant equation of state. Ind Eng Chem Fundam 1976;15. https://doi.org/10.1021/i160057a011.

[38] Juanes R, Spiteri EJ, Orr FM, Blunt MJ. Impact of relative permeability hysteresis on geological CO2 storage. Water Resour Res 2006;42(12). https://doi.org/10.1029/2005WR004806.

[39] Carlson FM. Simulation of relative permeability hysteresis to the nonwetting phase. In: SPE annual technical conference and exhibition. SPE Annual Technical Conference and Exhibition; 1981. https://doi.org/10.2118/10157-MS. SPE-10157-MS.

[40] Li Y-K, Nghiem LX. Phase equilibria of oil, gas and water/brine mixtures from a cubic equation of state and henry's law. Can J Chem Eng 1986;64(3):486–96. https://doi.org/10.1002/cjce.5450640319.

[41] Jossi JA, Stiel LI, Thodos G. The viscosity of pure substances in the dense gaseous and liquid phases. AIChE J 1962;8(1):59–63. https://doi.org/10.1002/aic.690080116.
[42] Duan Z, Mao S. A thermodynamic model for calculating methane solubility, density and gas phase composition of methane-bearing aqueous fluids from 273 to 523 K and from 1 to 2000 bar. Geochem Cosmochim Acta 2006;70(13):3369–86. https://doi.org/10.1016/j.gca.2006.03.018.
[43] Adebimpe AI, Foroughi S, Bijeljic B, Blunt MJ. Percolation without trapping: how Ostwald ripening during two-phase displacement in porous media alters capillary pressure and relative permeability. Phys Rev E 2024;110(3):035105. https://doi.org/10.1103/PhysRevE.110.035105.